

Fundamental measure theory of inhomogeneous two-body correlation functions

S. M. Tschopp and J. M. Brader

Department of Physics, University of Fribourg, CH-1700 Fribourg, Switzerland

For the three-dimensional hard-sphere model we investigate the inhomogeneous two-body correlations predicted by Rosenfeld’s fundamental measure theory. For the special cases in which the density has either planar or spherical symmetry we provide analytic formulae for the Hankel and Legendre transforms, respectively, of the inhomogeneous two-body direct correlation function as explicit functionals of the density. When combined with the Ornstein-Zernike relation our analytical results allow for rapid calculation of inhomogeneous hard-sphere density correlations in real-space. These provide not only information about the packing structures of the hard-sphere system, but also form an essential building-block for constructing perturbation theories of more realistic models.

I. INTRODUCTION

Two-body correlation functions give important information about the microstructural particle arrangement in a classical fluid. In the presence of an external field the density becomes nonuniform and the corresponding inhomogeneous two-body correlations can deviate significantly from those in bulk, e.g. for fluids at interfaces or under spatial confinement. For systems interacting via a pair potential these deviations provide direct access to interfacial thermodynamic quantities, such as the surface tension between coexisting phases [1–3].

The most familiar theoretical approach to calculating two-body correlations is the method of integral equations, based on closures of the Ornstein-Zernike (OZ) equation [4]. Approximations such as the Percus-Yevick (PY) or the hypernetted-chain have been widely used to study thermodynamics and two-body correlations in bulk [5], where translational invariance enables fast Fourier transform methods to be employed to great advantage in numerical calculations. For inhomogeneous systems this luxury is absent; the two-body correlation functions generally depend upon two vector arguments. However, for systems in which the density has a simple geometry (usually planar or spherical) the OZ equation can be reduced to a more manageable form. In such cases, generalizations of the bulk closure approximations have been used to calculate the inhomogeneous two-body correlations (see Refs.[6–8] for examples and chapter four in Ref.[2] for an overview).

An alternative approach is to use classical density functional theory (DFT). Within the DFT framework, correlation functions are generated by successive functional differentiation of the excess Helmholtz free energy functional with respect to the density. The functional contains complete statistical information about the system and can thus be used to calculate correlation functions of any order. Calculation of the inhomogeneous two-body correlations proceeds in the following way: (i) minimize the grand potential functional to obtain the equilibrium one-body density, (ii) evaluate the two-body direct correlation function (generated by taking two functional derivatives of the excess Helmholtz free energy) at the equilibrium density and then solve the OZ equation for

the two-body total correlation function. No closure is required, as the direct correlation function is uniquely specified by the generating functional. This two-step scheme, sometimes referred to as the ‘Ornstein-Zernike route’ is often used to obtain *bulk* two-body correlations (in which case the equilibrium density is a trivial constant), but is more rarely exploited to address inhomogeneous systems.

The most well-studied model in liquid-state theory is the hard-sphere system. In a classic 1989 paper Rosenfeld introduced a geometrically-based fundamental measure theory (FMT) density functional for hard-spheres [9]. The predictions of Rosenfeld FMT for the one-body density profile were found to be in excellent agreement with computer simulation data for a wide variety of external fields [10]. Although the original FMT encountered difficulties for strongly confined fluids and ordered states, subsequent versions of hard-sphere FMT corrected these shortcomings. The FMT, in common with other DFT approximations, is usually employed to obtain the equilibrium one-body density profile in a given external potential. Higher-body correlation functions are typically only evaluated in bulk [9] and *inhomogeneous* pair and higher-order correlation functions from FMT remain largely unexplored. This is perhaps surprising, given that the analytic formulae for the direct correlation functions present an obvious (and computationally advantageous) alternative to the inhomogeneous integral equation closures mentioned above. A deeper investigation of higher-order FMT correlation functions would not only provide insight into the structure of hard-sphere FMT, possibly suggesting improvements, but is also needed for the construction of perturbation theories aiming to describe more realistic inhomogeneous fluids.

In this paper we will address these issues and analyze in detail the inhomogeneous two-body correlations generated by FMT. We focus on situations for which the one-body density exhibits either planar or spherical symmetry and derive analytic formulae for the Hankel (planar geometry) and Legendre (spherical geometry) transforms of the inhomogeneous two-body FMT direct correlation function. These explicit functionals of the (one-dimensional) density profiles then provide rapid access to the direct and total pair correlation functions in real-space. Our results for hard-spheres will be tested against

the inhomogeneous PY integral equation theory and existing Monte-Carlo data. Once the quality of the FMT correlations has thus been established we will show how these can be exploited as input to a recently developed perturbative density functional theory for treating systems with attractive interactions [11].

The paper will be structured as follows: In Section II we briefly outline relevant aspects of classical DFT. In Section III we introduce the FMT and give explicit formulae for the Hankel and Legendre transforms of the two-body direct correlation function in planar and spherical geometry, respectively. In Section IV we present numerical results for the inhomogeneous total correlation function of hard-spheres confined between planar walls and in the presence of a fixed test particle. In Section V we show how our results for hard-spheres can be used as input to a perturbation theory of attractive interactions. In Section VI we give results obtained using this perturbation theory for the well-known hard-core Yukawa model. Finally, in Section VII, we discuss our findings and give an outlook for future investigations.

II. DENSITY FUNCTIONAL THEORY

DFT is an exact formalism for the study of classical many-body systems in external fields [1–3]. The central object of interest is the grand potential functional

$$\Omega[\rho] = F^{\text{id}}[\rho] + F^{\text{exc}}[\rho] - \int d\mathbf{r} (\mu - V_{\text{ext}}(\mathbf{r}))\rho(\mathbf{r}), \quad (1)$$

where μ is the chemical potential, $V_{\text{ext}}(\mathbf{r})$ is the external potential and $\rho(\mathbf{r})$ is the one-body ensemble averaged density. The square brackets indicate a functional dependence. The Helmholtz free energy of the ideal gas is exactly given by

$$F^{\text{id}}[\rho] = k_B T \int d\mathbf{r} \rho(\mathbf{r}) (\ln(\rho(\mathbf{r})) - 1), \quad (2)$$

where k_B is the Boltzmann constant, T is the temperature and we have set the thermal wavelength equal to unity. The excess Helmholtz free energy, F^{exc} , includes all information regarding the interparticle interactions and usually has to be approximated. The grand potential satisfies the variational condition

$$\frac{\delta\Omega[\rho]}{\delta\rho(\mathbf{r})} = 0. \quad (3)$$

This yields the following Euler-Lagrange equation for the equilibrium one-body density

$$\rho(\mathbf{r}) = e^{-\beta(V_{\text{ext}}(\mathbf{r}) - \mu - k_B T c^{(1)}(\mathbf{r}))}, \quad (4)$$

where the one-body direct correlation function is generated from the excess Helmholtz free energy by a functional derivative

$$c^{(1)}(\mathbf{r}) = -\frac{\delta\beta F^{\text{exc}}}{\delta\rho(\mathbf{r})}. \quad (5)$$

Substitution of the solution of (4) into (1) yields the equilibrium grand potential, thus providing access to all thermodynamic properties of the system.

Information about the two-body correlations in the inhomogeneous fluid can be obtained from a second functional derivative of the free energy

$$c^{(2)}(\mathbf{r}_1, \mathbf{r}_2) = -\frac{\delta^2\beta F^{\text{exc}}}{\delta\rho(\mathbf{r}_1)\delta\rho(\mathbf{r}_2)}, \quad (6)$$

where $c^{(2)}$ is the two-body direct correlation function. The connection between $c^{(2)}$ and the total correlation function, h , can be established by considering the functional derivative of equation (3) with respect to the external field

$$\frac{\delta^2\Omega}{\delta V_{\text{ext}}(\mathbf{r}_1)\delta\rho(\mathbf{r}_2)} = 0. \quad (7)$$

While the vanishing of this mixed derivative is a trivial consequence of (3), it is nevertheless a useful result. Explicit calculation of the left-hand side of (7) yields the OZ equation

$$h(\mathbf{r}_1, \mathbf{r}_2) = c^{(2)}(\mathbf{r}_1, \mathbf{r}_2) + \int d\mathbf{r}_3 h(\mathbf{r}_1, \mathbf{r}_3)\rho(\mathbf{r}_3)c^{(2)}(\mathbf{r}_3, \mathbf{r}_2), \quad (8)$$

Note that the external potential does not appear explicitly in the OZ equation, this information is implicitly contained within the one-body density.

III. HARD-SPHERES

Fundamental measure theory

We now focus our attention on a system of three-dimensional hard-spheres of radius R . Within FMT the excess Helmholtz free energy is approximated by an integral over a function of weighted densities [9]

$$\beta F_{\text{hs}}^{\text{exc}}[\rho] = \int d\mathbf{r}_1 \Phi(\{n_\alpha(\mathbf{r}_1)\}). \quad (9)$$

The original Rosenfeld formulation of FMT employs the following reduced excess free energy density

$$\Phi = -n_0 \ln(1 - n_3) + \frac{n_1 n_2 - \mathbf{n}_1 \cdot \mathbf{n}_2}{1 - n_3} + \frac{n_2^3 - 3n_2 \mathbf{n}_2 \cdot \mathbf{n}_2}{24\pi(1 - n_3)^2}. \quad (10)$$

The weighted densities are generated by convolution

$$n_\alpha(\mathbf{r}_1) = \int d\mathbf{r}_2 \rho(\mathbf{r}_2) \omega_\alpha(\mathbf{r}_1 - \mathbf{r}_2), \quad (11)$$

where the weight functions, ω_α , are characteristic of the geometry of the spheres. Of the six weight functions, four are scalars

$$\begin{aligned} \omega_3(\mathbf{r}) &= \Theta(R - r), & \omega_2(\mathbf{r}) &= \delta(R - r), \\ \omega_1(\mathbf{r}) &= \frac{\delta(R - r)}{4\pi R}, & \omega_0(\mathbf{r}) &= \frac{\delta(R - r)}{4\pi R^2}, \end{aligned}$$

and two are vectors

$$\omega_2(\mathbf{r}) = \mathbf{e}_r \delta(R-r), \quad \omega_1(\mathbf{r}) = \mathbf{e}_r \frac{\delta(R-r)}{4\pi R},$$

where $\mathbf{e}_r = \mathbf{r}/r$ is a unit vector. The presence of summations over both vector and scalar weights in many FMT expressions presents some notational difficulty and the analytical calculations below demand clarity regarding the scalar or vector character of various functions. We have thus chosen to employ the symbol ω for all weight functions, both scalar and vector, where the latter will be distinguished by employing a bold font index. This choice also enables us to use the convenient notation $\omega_{|\mathbf{2}|} = \omega_2$ and $\omega_{|\mathbf{1}|} = \omega_1$.

Applying the definition (5) to the free energy (9) generates the following approximate form for the one-body direct correlation function

$$c_{\text{hs}}^{(1)}(\mathbf{r}_1) = - \sum_{\alpha} \int d\mathbf{r}_2 \Phi'_{\alpha}(\mathbf{r}_2) \omega_{\alpha}(\mathbf{r}_{21}), \quad (12)$$

where $\Phi'_{\alpha} = \partial\Phi/\partial n_{\alpha}$, $\mathbf{r}_{21} = \mathbf{r}_2 - \mathbf{r}_1$ and the summation runs over all scalar and vector indices. Consistent with our established notation the function Φ'_{α} is a vector quantity when α takes the value $\mathbf{1}$ or $\mathbf{2}$, in which case a scalar product is implied in equation (12). While equation (12) makes an appearance in practically all FMT studies, the FMT approximation to the two-body direct correlation function is less frequently encountered and its general structure thus deserves some careful attention. Taking two functional derivatives of the free energy (9) generates the following expression

$$\begin{aligned} c_{\text{hs}}^{(2)}(\mathbf{r}_1, \mathbf{r}_2) &= - \sum_{\alpha\beta} \int d\mathbf{r}_3 \omega_{\alpha}(\mathbf{r}_{31}) \Phi''_{\alpha\beta}(\mathbf{r}_3) \omega_{\beta}(\mathbf{r}_{32}), \\ &\equiv - \sum_{\alpha\beta} c_{\alpha\beta}(\mathbf{r}_1, \mathbf{r}_2) \end{aligned} \quad (13)$$

where $\Phi''_{\alpha\beta} = \partial^2\Phi/\partial n_{\alpha}\partial n_{\beta}$. The terms, $c_{\alpha\beta}(\mathbf{r}_1, \mathbf{r}_2)$, contributing to the sum in (13), can be separated into three distinct classes according to the values of the α and β indices: 1. both scalars, 2. one scalar and one vector, and 3. both vectors. Each of these three classes involves a function $\Phi''_{\alpha\beta}$ of different tensorial rank (for convenience all first and second derivatives of Φ are given explicitly in Appendix A).

For terms belonging to class 1, the products in equation (13) are self-explanatory, as the second derivative $\Phi''_{\alpha\beta}$ and the weight functions are all scalars. For class 2 terms, we have one scalar weight, one vector weight and a vectorial second derivative function. A scalar product between the vector weight and $\Phi''_{\alpha\beta}$ is thus implied. For example, if $\alpha=2$ and $\beta=\mathbf{2}$ then the corresponding term in the sum (13) is given by

$$c_{22}(\mathbf{r}_1, \mathbf{r}_2) = \int d\mathbf{r}_3 \omega_2(\mathbf{r}_{31}) \Phi''_{22}(\mathbf{r}_3) \cdot \omega_2(\mathbf{r}_{32}).$$

For terms in class 3, we have two vector weights and $\Phi''_{\alpha\beta}$ is a second rank tensor. For example, the term with $\alpha=\mathbf{2}$ and $\beta=\mathbf{2}$ is given by a quadratic form

$$c_{22}(\mathbf{r}_1, \mathbf{r}_2) = \int d\mathbf{r}_3 \omega_2(\mathbf{r}_{31}) \cdot \Phi''_{22}(\mathbf{r}_3) \cdot \omega_2(\mathbf{r}_{32}).$$

The Helmholtz free energy density of the Rosenfeld FMT (10) is quadratic in the vector weighted densities. This has the simplifying consequence that $\Phi''_{\alpha\beta}$ for class 3 terms is proportional to the unit tensor. We note that this would generally not be the case for FMT approximations involving an extended set of weight functions (e.g. the Tarazona FMT [12]).

Inhomogeneous Percus-Yevick closure

An alternative approach to obtaining the inhomogeneous pair correlations is to supplement the OZ equation (8) by a second (usually local) closure relation between the pair direct correlation function and the total correlation function, and then to solve self-consistently the two coupled equations. A closure which is known to work well for hard-spheres is the PY approximation [4, 6, 13]

$$\begin{aligned} h_{\text{hs}}(\mathbf{r}_1, \mathbf{r}_2) &= -1 \quad \text{for } |\mathbf{r}_1 - \mathbf{r}_2| < 2R, \\ c_{\text{hs}}^{(2)}(\mathbf{r}_1, \mathbf{r}_2) &= 0 \quad \text{for } |\mathbf{r}_1 - \mathbf{r}_2| > 2R. \end{aligned} \quad (14)$$

The first of these relations is the exact ‘core condition’ reflecting the impossibility of hard-sphere overlaps. The PY theory can be solved exactly in bulk and yields an expression for the pair direct correlation function identical to that generated by the Rosenfeld FMT. However, as this agreement occurs only in bulk, care should be taken not to label the Rosenfeld FMT as the ‘PY functional’. For inhomogeneous situations the predictions of equation (13) for any given density profile will differ from the solution of the coupled equations (8) and (14). In particular, the FMT expression (13) will not satisfy exactly the core condition, although it may provide a good approximation. The PY theory has been shown to perform well in a variety of inhomogeneous situations [6–8] and we will thus use it as a benchmark for assessing the quality of the pair correlations generated by FMT.

FMT in planar geometry

When the external field has planar symmetry the density only varies as a function of a single cartesian coordinate, which we take to be the z -axis. The inhomogeneous pair correlations thus exhibit cylindrical symmetry and require as input two coordinates, z_1 and z_2 , and a cylindrical radial distance, r , separating them (see Fig.1). In this case the OZ equation (8) can be simplified using a Hankel transform (two dimensional Fourier transform) in

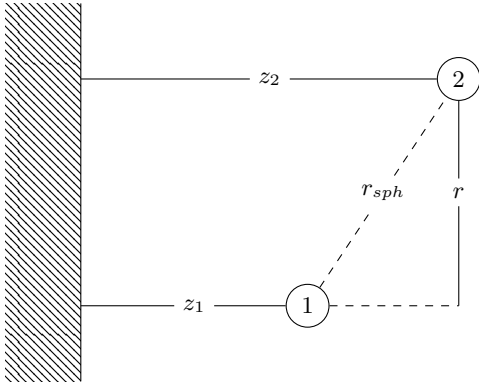


FIG. 1. Sketch of the planar geometry.

the plane orthogonal to z . The Hankel transform of the pair direct correlation function is given by

$$\bar{c}_{\text{hs}}^{(2)}(z_1, z_2, k) = 2\pi \int_0^\infty dr r J_0(kr) c_{\text{hs}}^{(2)}(z_1, z_2, r), \quad (15)$$

where k is the absolute value of the two-dimensional wavevector \mathbf{k} and J_0 is a Bessel function. The back-transform is given by

$$c_{\text{hs}}^{(2)}(z_1, z_2, r) = \frac{1}{2\pi} \int_0^\infty dk k J_0(kr) \bar{c}_{\text{hs}}^{(2)}(z_1, z_2, k). \quad (16)$$

Analogous expressions can be written for the total correlation function. Hankel transform of the OZ equation (8) yields (see Appendix B)

$$\begin{aligned} \bar{h}_{\text{hs}}(z_1, z_2, k) &= \bar{c}_{\text{hs}}^{(2)}(z_1, z_2, k) \\ &+ \int_{-\infty}^\infty dz_3 \bar{h}_{\text{hs}}(z_1, z_3, k) \rho(z_3) \bar{c}_{\text{hs}}^{(2)}(z_3, z_2, k). \end{aligned} \quad (17)$$

If ρ and $\bar{c}_{\text{hs}}^{(2)}$ are known functions, then (17) becomes a linear integral equation for the remaining unknown \bar{h}_{hs} .

Equation (13) gives the general FMT approximation to the pair direct correlation function as a functional of the three-dimensional density, but is not in a form suitable for numerical implementation. This is probably the reason why (13) has not been exploited for the development of liquid-state theory. In the following we will show that the Hankel transform of equation (13) can be reduced to an expression which allows for rapid and precise numerical evaluation of the pair correlations for any given planar density profile.

This ‘FMT route’ to the hard-sphere pair correlations is computationally efficient for a number of reasons: (i) The iterative solution of the linear integral equation (17) is both rapid and stable. (ii) The equations can be solved entirely in Hankel space with no need to back-transform to real-space during the iteration loop. (iii) The inhomogeneous pair correlation functions can be determined for a given value of k , independently of all other wavevectors. Calculations can thus be performed in parallel for

different k -values. It is worth to compare this comfortable situation with the demands of solving numerically the nonlinear PY integral equation theory (equations (8) and (14)) where we observe: (i) The iterative convergence rate is very slow at high densities and small Broyles mixing parameters must be employed to maintain stability [4, 10]. (ii) The OZ equation (17) is treated in Hankel space, whereas the closure (14) can only be implemented in real-space. This prevents parallel computation and demands an expensive back-and-forth Hankel transformation at each iteration step.

Hankel transform of the two-body direct correlation function (13) generates a sum of terms

$$\bar{c}_{\text{hs}}^{(2)}(z_1, z_2, k) = - \sum_{\alpha\beta} \bar{c}_{\alpha\beta}(z_1, z_2, k). \quad (18)$$

The main building blocks for each of the terms in (18) are the Hankel transformed scalar weight functions

$$\begin{aligned} \bar{w}_3(z_1, z_2, k) &= 2\pi \frac{R_{12}}{k} \Theta_{12} J_1(kR_{12}), \\ \bar{w}_2(z_1, z_2, k) &= 2\pi R \Theta_{12} J_0(kR_{12}), \\ \bar{w}_1(z_1, z_2, k) &= \frac{\bar{w}_2(z_1, z_2, k)}{4\pi R}, \\ \bar{w}_0(z_1, z_2, k) &= \frac{\bar{w}_2(z_1, z_2, k)}{4\pi R^2}, \end{aligned} \quad (19)$$

where $\Theta_{12} \equiv \Theta(R - |z_{12}|)$ is the Heaviside step function, $R_{12}^2 \equiv R^2 - z_{12}^2$ and $z_{12} = z_1 - z_2$.

In the discussion below equation (13) we identified three classes of terms appearing in the sum, grouped according to the values of the pair of indices α and β . For terms belonging to **class 1** the steps involved in transforming $c_{\alpha\beta}$ are identical to those required to transform the OZ equation (see Appendix B). This yields for $\alpha, \beta \in \{0, 1, 2, 3\}$ the following one-dimensional integral

$$\bar{c}_{\alpha\beta}(z_1, z_2, k) = \int_a^b dz_3 \bar{w}_\alpha(z_3, z_1, k) \Phi''_{\alpha\beta}(z_3) \bar{w}_\beta(z_3, z_2, k), \quad (20)$$

for $|z_{12}| \leq 2R$ and zero otherwise. The integration limits are a consequence of the finite range of the weight functions and are given by $a = \max(z_1, z_2) - R$ and $b = \min(z_1, z_2) + R$, respectively.

The mixed terms belonging to **class 2** have one scalar and one vector index. For example, if we have $\alpha \in \{0, 1, 2, 3\}$ and $\beta \in \{1, 2\}$, then we must consider the following scalar product

$$\Phi''_{\alpha\beta}(z_3) \cdot \omega_\beta(\mathbf{r}_{32}) = |\Phi''_{\alpha\beta}(z_3)| \omega_{|\beta|}(\mathbf{r}_{32}) \mathbf{e}_{z_3} \cdot \mathbf{e}_{32}^{\text{shell}},$$

where we define an (outwards pointing) unit vector, orthogonal to the surface of the spherical delta-shell centered at \mathbf{r}_2 :

$$\mathbf{e}_{32}^{\text{shell}} = \begin{cases} \frac{\mathbf{r}_3 - \mathbf{r}_2}{R} & |\mathbf{r}_3 - \mathbf{r}_2| = R, \\ 0 & \text{otherwise.} \end{cases} \quad (21)$$

The scalar product is obtained by simple trigonometry, $\mathbf{e}_{z_3} \cdot \mathbf{e}_{32}^{\text{shell}} = z_{32}/R$. As this result depends only on z_3 and z_2 its presence in the integrand of (13) does not interfere with the Hankel transformation and the standard procedure outlined in Appendix B can be applied without modification. We thus obtain the following expression

$$\bar{c}_{\alpha\beta}(z_1, z_2, k) = \frac{1}{R} \int_a^b dz_3 \bar{\omega}_\alpha(z_3, z_1, k) |\Phi''_{\alpha\beta}(z_3)| \times z_{32} \bar{\omega}_{|\beta|}(z_3, z_2, k), \quad (22)$$

for $|z_{12}| \leq 2R$ and zero otherwise. The same considerations apply when the rank of the indices is exchanged, $\alpha \in \{1, 2\}$ and $\beta \in \{0, 1, 2, 3\}$. This yields

$$\bar{c}_{\alpha\beta}(z_1, z_2, k) = \frac{1}{R} \int_a^b dz_3 \bar{\omega}_{|\alpha|}(z_3, z_1, k) z_{31} \times |\Phi''_{\alpha\beta}(z_3)| \bar{\omega}_\beta(z_3, z_2, k), \quad (23)$$

for $|z_{12}| \leq 2R$ and zero otherwise.

Terms in **class 3** have a product of two vector weight functions, $\alpha, \beta \in \{1, 2\}$, and are more difficult to deal with. For the original FMT used in this work the second derivative tensor can be expressed as $\Phi''_{\alpha\beta} \equiv \tilde{\Phi}''_{\alpha\beta} \mathbb{1}$, where $\tilde{\Phi}''_{\alpha\beta}$ is a scalar function and $\mathbb{1}$ is the unit tensor. This enables us to simplify the quadratic form in the integrand of $\bar{c}_{\alpha\beta}$ to a scalar product between unit vectors

$$\omega_\alpha(\mathbf{r}_{31}) \cdot \Phi''_{\alpha\beta}(z_3) \cdot \omega_\beta(\mathbf{r}_{32}) = \tilde{\Phi}''_{\alpha\beta}(z_3) \omega_{|\alpha|}(\mathbf{r}_{31}) \omega_{|\beta|}(\mathbf{r}_{32}) \mathbf{e}_{31}^{\text{shell}} \cdot \mathbf{e}_{32}^{\text{shell}}. \quad (24)$$

In Fig.2 we sketch the intersection of a pair of delta-shells centered at \mathbf{r}_1 and \mathbf{r}_2 , representing a product of weight functions $\omega_\alpha(\mathbf{r}_{31}) \omega_\beta(\mathbf{r}_{32})$ for $\alpha, \beta \in \{1, 2\}$. The values of the integration variable \mathbf{r}_3 which yield a nonzero contribution to (24) lie on the intersection circle of the delta-shells. For such cases the points \mathbf{r}_1 , \mathbf{r}_2 and \mathbf{r}_3 define an isosceles triangle with fixed angles. If we choose z_1 as

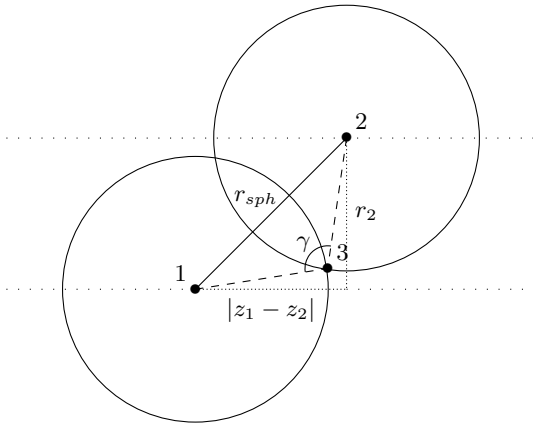


FIG. 2. Geometrical sketch for evaluation of the scalar product given in (25).

the axis of our cylindrical coordinate system then it is a straightforward geometrical exercise to show that for \mathbf{r}_3 anywhere on the intersection circle

$$\mathbf{e}_{31}^{\text{shell}} \cdot \mathbf{e}_{32}^{\text{shell}} \equiv \cos(\gamma) = 1 - \frac{z_{12}^2}{2R^2} - \frac{r_2^2}{2R^2}, \quad (25)$$

where γ is defined in Fig.2. Due to our identification of z_1 with the cylindrical coordinate axis the variable r_1 does not appear in (25). We thus seek to evaluate the Hankel transform of

$$c_{\alpha\beta}(z_1, z_2, r_2) = c_{\alpha\beta}^A(z_1, z_2, r_2) + c_{\alpha\beta}^B(z_1, z_2, r_2) \quad (26)$$

where the two contributions are given by

$$c_{\alpha\beta}^A(z_1, z_2, r_2) = \int d\mathbf{r}_3 \tilde{\Phi}''_{\alpha\beta}(z_3) \omega_{|\alpha|}(\mathbf{r}_{31}) \omega_{|\beta|}(\mathbf{r}_{32}) \left(1 - \frac{z_{12}^2}{2R^2}\right),$$

$$c_{\alpha\beta}^B(z_1, z_2, r_2) = - \int d\mathbf{r}_3 \tilde{\Phi}''_{\alpha\beta}(z_3) \omega_{|\alpha|}(\mathbf{r}_{31}) \omega_{|\beta|}(\mathbf{r}_{32}) \left(\frac{r_2^2}{2R^2}\right).$$

The factor $1 - z_{12}^2/2R^2$ appearing in the first of these contributions is independent of the radial coordinate. The Hankel transformation of $c_{\alpha\beta}^A$ thus proceeds in the same way as for the OZ equation (see Appendix B) and yields

$$\bar{c}_{\alpha\beta}^A(z_1, z_2, k) = \left(1 - \frac{z_{12}^2}{2R^2}\right) \mathcal{A}_{\alpha\beta}(z_1, z_2, k), \quad (27)$$

for $|z_{12}| \leq 2R$ and zero otherwise, where the function $\mathcal{A}_{\alpha\beta}$ is given by

$$\mathcal{A}_{\alpha\beta}(z_1, z_2, k) = \int_a^b dz_3 \tilde{\Phi}''_{\alpha\beta}(z_3) \bar{\omega}_{|\alpha|}(z_3, z_1, k) \bar{\omega}_{|\beta|}(z_3, z_2, k).$$

Hankel transform of $c_{\alpha\beta}^B$ is complicated by the presence of the factor r_2^2 . Following again the procedure outlined in Appendix B, we find that the first step of the calculation can be carried through easily, leading to

$$c_{\alpha\beta}^B(z_1, z_2, r_2) = - \frac{r_2^2}{4\pi R^2} \int_a^b dz_3 \tilde{\Phi}''_{\alpha\beta}(z_3) \times \int_0^\infty dk' k' \bar{\omega}_\alpha(z_3, z_1, k') \bar{\omega}_\beta(z_3, z_2, k') J_0(k' r_2). \quad (28)$$

It is the second step of the calculation (Hankel transformation with respect to the external coordinate r_2) which presents difficulties. Applying the integral operator $2\pi \int_0^\infty dr_2 r_2 J_0(kr_2)$ to (28) yields the Hankel transformation

$$\bar{c}_{\alpha\beta}^B(z_1, z_2, k) = \frac{1}{4\pi R^2} \int_a^b dz_3 \tilde{\Phi}''_{\alpha\beta}(z_3) \int_0^\infty dk' k' \bar{\omega}_\alpha(z_3, z_1, k') \times \bar{\omega}_\beta(z_3, z_2, k') \left[2\pi \int_0^\infty dr_2 r_2 J_0(kr_2) (-r_2^2 J_0(k' r_2)) \right]. \quad (29)$$

To make progress we must evaluate the integral in square brackets; the Hankel transform of $-r_2^2 J_0(k'r_2)$. Given a test function, $f(r)$, which vanishes sufficiently rapidly as $r \rightarrow \infty$, it can be shown that the Hankel transform of $-r^2 f(r)$ is given by

$$\overline{-r^2 f(r)} = \frac{d^2 \bar{f}(k)}{dk^2} + \frac{1}{k} \frac{d\bar{f}(k)}{dk}. \quad (30)$$

Setting $f(r) = J_0(k'r)$ and using the result (B8) yields

$$\overline{-r_2^2 J_0(k'r_2)} = (2\pi)^2 \left(\delta''(\mathbf{k} - \mathbf{k}') + \frac{1}{k} \delta'(\mathbf{k} - \mathbf{k}') \right), \quad (31)$$

where the prime(s) on the δ -functions express the first(second) derivative with respect to k . Using the known properties of delta-function derivatives the expression (29) thus becomes

$$\begin{aligned} \bar{c}_{\alpha\beta}^B(z_1, z_2, k) &= \frac{2\pi^2}{(4\pi R)^{\delta_{1|\alpha|} + \delta_{1|\beta|}}} \int_a^b dz_3 \tilde{\Phi}_{\alpha\beta}''(z_3) \quad (32) \\ &\times \left(\frac{\partial^2}{\partial k^2} + \frac{1}{k} \frac{\partial}{\partial k} \right) \left(J_0(kR_{13}) J_0(kR_{23}) \right), \end{aligned}$$

where we have used the explicit expressions for the transformed weight functions (19) to introduce the Bessel functions. The derivatives of the Bessel function product yield the following expression

$$\begin{aligned} &\left(\frac{\partial^2}{\partial k^2} + \frac{1}{k} \frac{\partial}{\partial k} \right) \left(J_0(kR_{13}) J_0(kR_{23}) \right) = \quad (33) \\ &-\frac{1}{2} (R_{13}^2 + R_{23}^2) J_0(kR_{13}) J_0(kR_{23}) \\ &+ 2R_{13}R_{23} J_1(kR_{13}) J_1(kR_{23}) \\ &+ \frac{1}{2} R_{13}^2 J_2(kR_{13}) J_0(kR_{23}) + \frac{1}{2} R_{23}^2 J_0(kR_{13}) J_2(kR_{23}) \\ &- \frac{1}{k} \left(R_{13} J_1(kR_{13}) J_0(kR_{23}) + R_{23} J_0(kR_{13}) J_1(kR_{23}) \right). \end{aligned}$$

Putting the results (32) and (33) together with (26) and (27) yields the final result for the Hankel transform of the class 3 contributions with $\alpha, \beta \in \{1, 2\}$

$$\begin{aligned} \bar{c}_{\alpha\beta}(z_1, z_2, k) &= \left(1 - \frac{z_{12}^2}{2R^2} \right) \mathcal{A}_{\alpha\beta}(z_1, z_2, k) \\ &+ \frac{2\pi^2}{(4\pi R)^{\delta_{1|\alpha|} + \delta_{1|\beta|}}} \mathcal{B}_{\alpha\beta}(z_1, z_2, k), \quad (34) \end{aligned}$$

for $|z_{12}| \leq 2R$ and zero otherwise, where

$$\begin{aligned} \mathcal{B}_{\alpha\beta}(z_1, z_2, k) &= \int_a^b dz_3 \tilde{\Phi}_{\alpha\beta}''(z_3) \\ &\times \left\{ -\frac{R_{13}^2 + R_{23}^2}{2} J_0(kR_{13}) J_0(kR_{23}) \right. \\ &+ 2R_{13}R_{23} J_1(kR_{13}) J_1(kR_{23}) + \frac{R_{13}^2}{2} J_2(kR_{13}) J_0(kR_{23}) \\ &+ \frac{R_{23}^2}{2} J_0(kR_{13}) J_2(kR_{23}) - \frac{1}{k} \left(R_{13} J_1(kR_{13}) J_0(kR_{23}) \right. \\ &\left. \left. + R_{23} J_0(kR_{13}) J_1(kR_{23}) \right) \right\}. \end{aligned}$$

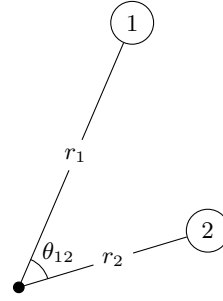


FIG. 3. Sketch of the spherical geometry.

To summarize, equations (18), (20), (22), (23), and (34) provide the Hankel transform of the FMT pair direct correlation function as an explicit functional of the one-dimensional planar density profile. Given $\bar{c}_{\text{hs}}^{(2)}$ the total correlation function, \bar{h}_{hs} can be calculated using the OZ relation (17). The pair correlations in real-space can then be obtained via (numerical) Hankel back-transformation using (16).

FMT in spherical geometry

When the external field has spherical symmetry the density only varies as a function of the distance from the origin. The inhomogeneous pair correlations thus require as input the two radial distances, r_1 and r_2 , and the cosine of the angle between them, $x_{12} = \cos(\theta_{12})$ (see Fig.3). In planar geometry the transformed weight functions (19) depend only on the separation z_{12} , whereas the analogous expressions in spherical geometry depend on both arguments r_1 and r_2 . In addition, the transformed weight functions in spherical geometry change their functional forms whenever one (or both) of these arguments approaches the origin to within a distance R . With the intention of sparing the reader technical overload, the results to be presented below will be restricted to cases satisfying both $r_1 \geq R$ and $r_2 \geq R$. If other situations arise, as would be the case for e.g. hard-spheres confined to a spherical cavity, then the methods to be discussed below could be easily generalized. In the following we will consider only test-particle calculations, for which the density, $\rho(r)$, is zero for $r < R$.

The Legendre transform of the pair direct correlation function is given by

$$\hat{c}_{\text{hs}}^{(2)}(r_1, r_2, n) = \frac{2n+1}{2} \int_{-1}^1 dx_{12} P_n(x_{12}) c_{\text{hs}}^{(2)}(r_1, r_2, x_{12}), \quad (35)$$

where $P_n(x_{12})$ is a Legendre polynomial. The back-transform is given by

$$c_{\text{hs}}^{(2)}(r_1, r_2, x_{12}) = \sum_{n=0}^{\infty} P_n(x_{12}) \hat{c}_{\text{hs}}^{(2)}(r_1, r_2, n). \quad (36)$$

Legendre transform of the OZ equation (8) simplifies the three-dimensional integral and yields the following equation for the transforms (see Appendix C)

$$\begin{aligned} \hat{h}_{\text{hs}}(r_1, r_2, n) &= \hat{c}_{\text{hs}}^{(2)}(r_1, r_2, n) \\ &+ \frac{4\pi}{2n+1} \int_0^\infty dr_3 r_3^2 \hat{h}_{\text{hs}}(r_1, r_3, n) \rho(r_3) \hat{c}_{\text{hs}}^{(2)}(r_3, r_2, n). \end{aligned} \quad (37)$$

The Legendre transform of the two-body direct correlation function (13) can be expressed as the following sum

$$\hat{c}_{\text{hs}}^{(2)}(r_1, r_2, n) = - \sum_{\alpha\beta} \hat{c}_{\alpha\beta}(r_1, r_2, n), \quad (38)$$

where the terms in (38) are constructed using the Legendre transformed scalar weight functions

$$\begin{aligned} \hat{\omega}_3(r_1, r_2, n) &= \begin{cases} \frac{1}{2}(1-x_{12})\Theta_{12} & n=0, \\ \frac{3}{4}(1-x_{12}^2)\Theta_{12} & n=1, \\ \frac{2n+1}{2n}(x_{12}P_n(x_{12})-P_{n+1}(x_{12}))\Theta_{12} & n \geq 2, \end{cases} \\ \hat{\omega}_2(r_1, r_2, n) &= \frac{2n+1}{2} \frac{R}{r_1 r_2} P_n(x_{12})\Theta_{12}, \\ \hat{\omega}_1(r_1, r_2, n) &= \frac{\hat{\omega}_2(r_1, r_2, n)}{4\pi R}, \\ \hat{\omega}_0(r_1, r_2, n) &= \frac{\hat{\omega}_2(r_1, r_2, n)}{4\pi R^2}, \end{aligned} \quad (39)$$

where $x_{12} = (r_1^2 + r_2^2 - R^2)/(2r_1 r_2)$, $\Theta_{12} \equiv \Theta(R - |r_{12}|)$ is the Heaviside step function and $r_{12} = r_1 - r_2$.

In analogy with our treatment of planar geometry we consider separately the three classes of terms contributing to the sum (38). For terms belonging to **class 1** the steps involved in transforming $c_{\alpha\beta}$ are identical to those required to transform the OZ equation (see Appendix C). For $\alpha, \beta \in \{0, 1, 2, 3\}$ this yields

$$\begin{aligned} \hat{c}_{\alpha\beta}(r_1, r_2, n) &= \frac{4\pi}{2n+1} \int_d^e dr_3 r_3^2 \\ &\times \hat{\omega}_\alpha(r_3, r_1, n) \Phi''_{\alpha\beta}(r_3) \hat{\omega}_\beta(r_3, r_2, n), \end{aligned} \quad (40)$$

for $|r_{12}| \leq 2R$ and zero otherwise. For the restricted ranges of r_1 and r_2 under consideration the integration limits are $d = \max(r_1, r_2) - R$ and $e = \min(r_1, r_2) + R$.

For mixed terms with $\alpha \in \{0, 1, 2, 3\}$ and $\beta \in \{1, 2\}$, we consider the following scalar product

$$\Phi''_{\alpha\beta}(r_3) \cdot \omega_\beta(\mathbf{r}_{32}) = |\Phi''_{\alpha\beta}(r_3)| \omega_{|\beta|}(\mathbf{r}_{32}) \mathbf{e}_{r_3} \cdot \mathbf{e}_{32}^{\text{shell}},$$

where $\mathbf{e}_{r_3} \cdot \mathbf{e}_{32}^{\text{shell}} = (R^2 + r_3^2 - r_2^2)/(2r_3 R)$. This result depends only on r_3 and r_2 and so its presence in the integrand does not interfere with the Legendre transformation and the standard procedure given in Appendix C can be applied without modification. We thus obtain the following expression

$$\begin{aligned} \hat{c}_{\alpha\beta}(r_1, r_2, n) &= \frac{4\pi}{2n+1} \int_d^e dr_3 r_3^2 \hat{\omega}_\alpha(r_3, r_1, n) |\Phi''_{\alpha\beta}(r_3)| \\ &\times \left(\frac{R^2 + r_3^2 - r_2^2}{2r_3 R} \right) \hat{\omega}_{|\beta|}(r_3, r_2, n), \end{aligned} \quad (41)$$

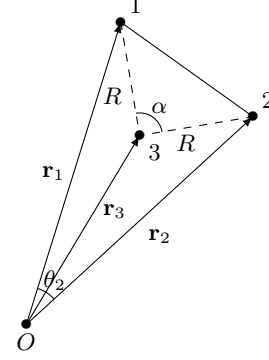


FIG. 4. Geometrical sketch for evaluation of the scalar product given in (44). We orient our spherical coordinate system such that the z -axis lies along \mathbf{r}_1 .

for $|r_{12}| \leq 2R$ and zero otherwise. Similarly, when the rank of the indices is exchanged, $\alpha \in \{1, 2\}$ and $\beta \in \{0, 1, 2, 3\}$, we find

$$\begin{aligned} \hat{c}_{\alpha\beta}(r_1, r_2, n) &= \frac{4\pi}{2n+1} \int_d^e dr_3 r_3^2 \hat{\omega}_{|\alpha|}(r_3, r_1, n) \\ &\times \left(\frac{R^2 + r_3^2 - r_1^2}{2r_3 R} \right) |\Phi''_{\alpha\beta}(r_3)| \hat{\omega}_\beta(r_3, r_2, n), \end{aligned} \quad (42)$$

for $|r_{12}| \leq 2R$ and zero otherwise.

As in the planar case, the terms in **class 3** are more difficult to deal with and we must consider the following scalar product

$$\begin{aligned} \omega_\alpha(\mathbf{r}_{31}) \cdot \Phi''_{\alpha\beta}(r_3) \cdot \omega_\beta(\mathbf{r}_{32}) &= \\ \tilde{\Phi}''_{\alpha\beta}(r_3) \omega_{|\alpha|}(\mathbf{r}_{31}) \omega_{|\beta|}(\mathbf{r}_{32}) \mathbf{e}_{31}^{\text{shell}} \cdot \mathbf{e}_{32}^{\text{shell}}. \end{aligned} \quad (43)$$

In Fig.4 we sketch the three vectors \mathbf{r}_1 , \mathbf{r}_2 and \mathbf{r}_3 . The values of \mathbf{r}_3 which yield a nonzero contribution to (43) lie on the intersection circle of delta-shells centered at \mathbf{r}_1 and \mathbf{r}_2 . If we choose \mathbf{r}_1 along the z -axis of our spherical coordinate system, then for \mathbf{r}_3 anywhere on the intersection circle we find

$$\mathbf{e}_{31}^{\text{shell}} \cdot \mathbf{e}_{32}^{\text{shell}} \equiv \cos(\alpha) = 1 - \frac{r_1^2 + r_2^2}{2R^2} + \frac{r_1 r_2}{R^2} P_1(x_2), \quad (44)$$

where the angle α is defined in Fig.4 and $x_2 = \cos(\theta_2)$. We thus seek to evaluate the Legendre transform of

$$c_{\alpha\beta}(r_1, r_2, x_2) = c_{\alpha\beta}^D(r_1, r_2, x_2) + c_{\alpha\beta}^E(r_1, r_2, x_2), \quad (45)$$

where the two contributions are given by

$$\begin{aligned} c_{\alpha\beta}^D(r_1, r_2, x_2) &= \int d\mathbf{r}_3 \tilde{\Phi}''_{\alpha\beta}(r_3) \\ &\times \omega_{|\alpha|}(\mathbf{r}_{31}) \omega_{|\beta|}(\mathbf{r}_{32}) \left(1 - \frac{r_1^2 + r_2^2}{2R^2} \right), \\ c_{\alpha\beta}^E(r_1, r_2, x_2) &= \int d\mathbf{r}_3 \tilde{\Phi}''_{\alpha\beta}(r_3) \\ &\times \omega_{|\alpha|}(\mathbf{r}_{31}) \omega_{|\beta|}(\mathbf{r}_{32}) \left(\frac{r_1 r_2}{R^2} P_1(x_2) \right). \end{aligned}$$

The factor $1 - (r_1^2 + r_2^2)/(2R^2)$ is independent of x_2 and Legendre transformation thus proceeds in the same way as for the OZ equation (see Appendix C). This yields

$$\hat{c}_{\alpha\beta}^D(r_1, r_2, n) = \left(1 - \frac{r_1^2 + r_2^2}{2R^2}\right) \mathcal{D}_{\alpha\beta}(r_1, r_2, n), \quad (46)$$

for $|r_{12}| \leq 2R$ and zero otherwise, where the function $\mathcal{D}_{\alpha\beta}$ is given by

$$\begin{aligned} \mathcal{D}_{\alpha\beta}(r_1, r_2, n) &= \frac{4\pi}{2n+1} \int_0^\infty dr_3 r_3^2 \\ &\times \tilde{\Phi}_{\alpha\beta}''(r_3) \hat{\omega}_{|\alpha|}(r_3, r_1, n) \hat{\omega}_{|\beta|}(r_3, r_2, n). \end{aligned}$$

Legendre transform of $c_{\alpha\beta}^E$ is more difficult due to the presence of the factor $P_1(x_2)$. If we follow the procedure of Appendix C we find that the first step of the calculation can be carried through easily to obtain

$$\begin{aligned} c_{\alpha\beta}^E(r_1, r_2, x_2) &= 2\pi \int_0^\infty dr_3 r_3^2 \tilde{\Phi}_{\alpha\beta}''(r_3) \\ &\times \sum_{i=0}^\infty \frac{2}{2i+1} \hat{\omega}_{|\alpha|}(r_3, r_1, i) \hat{\omega}_{|\beta|}(r_3, r_2, i) \frac{r_1 r_2}{R^2} P_1(x_2) P_i(x_2). \end{aligned} \quad (47)$$

Applying the operator $\frac{2n+1}{2} \int_{-1}^1 dx_2 P_n(x_2)$ to (47) then yields the Legendre transformation

$$\begin{aligned} \hat{c}_{\alpha\beta}^E(r_1, r_2, n) &= 2\pi \frac{2n+1}{2} \int_0^\infty dr_3 r_3^2 \tilde{\Phi}_{\alpha\beta}''(r_3) \\ &\times \sum_{i=0}^\infty \frac{2}{2i+1} \hat{\omega}_{|\alpha|}(r_3, r_1, i) \hat{\omega}_{|\beta|}(r_3, r_2, i) \\ &\times \frac{r_1 r_2}{R^2} \int_{-1}^1 dx_2 P_1(x_2) P_n(x_2) P_i(x_2). \end{aligned} \quad (48)$$

The extra complication here is caused by the integral of a triple product of Legendre polynomials. Fortunately, this integration has been well-studied in the context of quantum mechanics and can be reexpressed using the Wigner $3j$ notation (see e.g. [14])

$$\int_{-1}^1 dx_2 P_l(x_2) P_n(x_2) P_i(x_2) = 2 \begin{pmatrix} l & n & i \\ 0 & 0 & 0 \end{pmatrix}^2. \quad (49)$$

For the case of interest here, $l=1$, there are only two terms in the sum over i appearing in (48). This leads to the result

$$\hat{c}_{\alpha\beta}^E(r_1, r_2, n) = \frac{r_1 r_2}{R^2} \mathcal{E}_{\alpha\beta}(r_1, r_2, n), \quad (50)$$

for $|r_{12}| \leq 2R$ and zero otherwise, where

$$\begin{aligned} \mathcal{E}_{\alpha\beta}(r_1, r_2, n) &= \frac{4\pi}{2n+1} \int_0^\infty dr_3 r_3^2 \tilde{\Phi}_{\alpha\beta}''(r_3) \\ &\times \left(\frac{n(2n+1)}{(2n-1)^2} \hat{\omega}_{|\alpha|}(r_3, r_1, n-1) \hat{\omega}_{|\beta|}(r_3, r_2, n-1) \right. \\ &\left. + \frac{(n+1)(2n+1)}{(2n+3)^2} \hat{\omega}_{|\alpha|}(r_3, r_1, n+1) \hat{\omega}_{|\beta|}(r_3, r_2, n+1) \right). \end{aligned} \quad (51)$$

Putting together (45), (46) and (50) yields the final result for the Legendre transform of the class 3 contributions with $\alpha, \beta \in \{\mathbf{1}, \mathbf{2}\}$

$$\begin{aligned} \hat{c}_{\alpha\beta}(r_1, r_2, n) &= \left(1 - \frac{r_1^2 + r_2^2}{2R^2}\right) \mathcal{D}_{\alpha\beta}(r_1, r_2, n) \\ &+ \frac{r_1 r_2}{R^2} \mathcal{E}_{\alpha\beta}(r_1, r_2, n), \end{aligned} \quad (52)$$

for $|r_{12}| \leq 2R$ and zero otherwise. In summary, equations (38), (40), (41), (42), and (52) provide the Legendre transform of the FMT pair direct correlation function, $\hat{c}_{\text{hs}}^{(2)}$, as an explicit functional of the one-dimensional spherical density profile, $\rho(r)$.

Numerical consistency checks

The formulae presented in the previous subsections for the Hankel and Legendre transforms of the pair direct correlation functions are, in principle, straightforward to implement. However, when developing numerics to evaluate the remaining one-dimensional integrals it is useful to have some checks and limiting cases to help eliminate possible coding errors. In bulk there are two helpful benchmarks: (i) In the low density limit the pair direct correlation function reduces to the Mayer function [4] for which both the Hankel and Legendre transforms are known exactly. (ii) At finite density the (real-space) analytic expression for the PY pair direct correlation function [4] can be numerically Hankel/Legendre transformed using (15) and (35), respectively. The result thus obtained should agree with the predictions of our analytical expressions. Contributions arising from class 2 terms (scalar-vector combinations) vanish in bulk and can thus only be tested by considering inhomogeneous density profiles. A useful check is the following relation between the one- and two-body direct correlation functions

$$\nabla_1 c^{(1)}(\mathbf{r}_1) = \int d\mathbf{r}_2 c^{(2)}(\mathbf{r}_1, \mathbf{r}_2) \nabla_2 \rho(\mathbf{r}_2), \quad (53)$$

known as the Lovett-Mou-Buff-Wertheim sum-rule [3]. In planar geometry this reduces to

$$\frac{\partial c^{(1)}(z_1)}{\partial z_1} = \int_{-\infty}^\infty dz_2 \frac{\partial \rho(z_2)}{\partial z_2} \bar{c}^{(2)}(z_1, z_2, k=0), \quad (54)$$

where both $c^{(1)}$ and $c^{(2)}$ are evaluated at the equilibrium density, ρ . In spherical geometry equation (53) becomes

$$\frac{\partial \hat{c}^{(1)}(r_1)}{\partial r_1} = \frac{4\pi}{3} \int_0^\infty dr_2 r_2^2 \frac{\partial \rho(r_2)}{\partial r_2} \hat{c}(r_1, r_2, n=1). \quad (55)$$

Finally, in planar geometry a transverse structure factor can be defined as [1]

$$H(z_1, k) \equiv 1 + \int dz_2 \bar{h}(z_1, z_2, k) \rho(z_2) \quad (56)$$

$$= 1 + \int dz_2 H(z_2, k) \rho(z_2) \bar{c}^{(2)}(z_2, z_1, k), \quad (57)$$

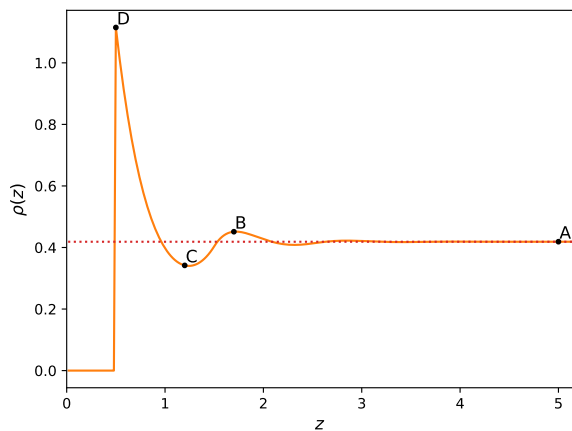


FIG. 5. **Hard-spheres at a hard-wall.** Density profile for $\mu = 2$ (solid line) with its plateau value indicated (horizontal dotted line). Points indicate the z -coordinates for which we show the total correlation function in Fig.6.

where the second equality is an integral equation requiring iterative solution. The transverse structure factor is related to the local compressibility according to

$$H(z, k=0) = \frac{1}{\beta\rho(z)} \frac{\partial\rho(z)}{\partial\mu}. \quad (58)$$

Satisfying equations (56) and (58) provides an additional check that the numerical solution of the OZ equation (17) for \hat{h}_{hs} has been performed correctly.

IV. RESULTS FOR HARD-SPHERES

Planar geometry

In Fig.5 we show a FMT density profile for hard-spheres at a hard-wall. The chosen value of the chemical potential ($\mu=2$) corresponds to a liquid-state of intermediate bulk density. In the vicinity of the wall we observe the familiar packing oscillations which then decay rapidly into the bulk. The four points marked on the curve indicate the positions at which we will investigate the inhomogeneous two-body correlations. When analyzing two-body correlations with planar symmetry we are faced with a function of three independent scalar arguments. This naturally presents many alternatives for graphical representation of the data. Following a quite extensive study of these various possibilities we have come to the conclusion that simple one-dimensional plots showing the variation of the correlation functions as a function of r for equal values of the z -coordinates provides a reasonable way to compare different theories. Similar plots for fixed, but distinct, values of the z -coordinates were not found to offer any greater insight.

In Fig.6, we show the total correlation function for $z_1 = z_2 = z$ as a function of the cylindrical radial coordinate, r . In each panel we indicate the bulk function,

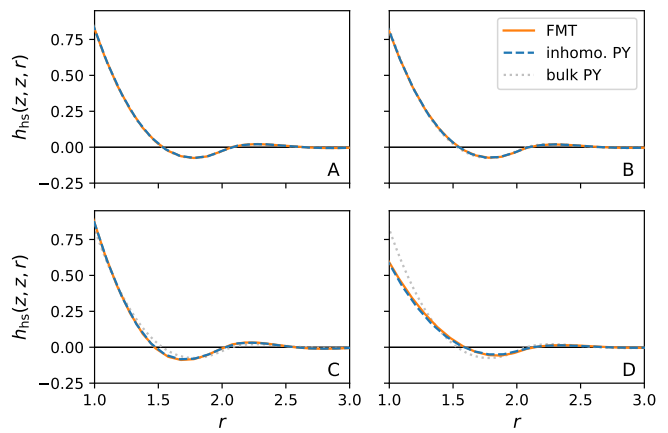


FIG. 6. **Hard-spheres at a hard-wall.** Total correlation function for equal values of the two z -arguments, $h_{\text{hs}}(z, z, r)$, corresponding to the z -positions indicated on the density profile shown in Fig.5. FMT (full orange line), inhomogeneous PY (dashed blue line) and PY bulk solution (grey dotted line). At points A and B all three curves remain essentially identical. At points C and D there are deviations from bulk, but excellent agreement between FMT and PY theory.

$h_{\text{hs}}(z \rightarrow \infty, z \rightarrow \infty, r)$, as a visual reference. Moving through the panels from A to D we observe increasing deviation of the inhomogeneous total correlation function from its bulk form. At all of the considered points the FMT prediction stays very close to that of the inhomogeneous PY theory, even when the density is strongly varying. This good level of agreement between the PY theory and FMT gives us some confidence in the quality of FMT at the two-body level, at least for these intermediate densities. We note that the PY total correlation function of hard-spheres is unique, in the sense that it is generated by a strictly truncated direct correlation for $r_{12} > 1$ while still satisfying the core condition (see (14)). Due to the finite range of the weight functions the FMT direct correlation function automatically satisfies the first of these conditions, but not the second (except in the low density limit). It thus follows that any deviation of the FMT total correlation function from the PY theory is a consequence of core condition violation. The good level of agreement shown in Fig.6 can be therefore taken as an indirect indication that the core condition is well approximated by FMT for the considered density.

We next consider a more demanding case: densely packed hard-spheres confined between two parallel hard-walls separated by four particle diameters. In Fig.7 we show the density calculated at $\mu = 5$, which generates a strongly inhomogeneous profile. The points label the positions at which we will investigate the inhomogeneous total correlation function. In Fig.8 we show h_{hs} as a function of r for $z = 1$ and $z = 0.5$ (the positions labelled C and D in Fig.7). At the point C, close to the first minimum of the profile, we find very close agreement between the PY theory and FMT, with only slight deviation at around $r = 1.75$. At point D, corresponding to the con-

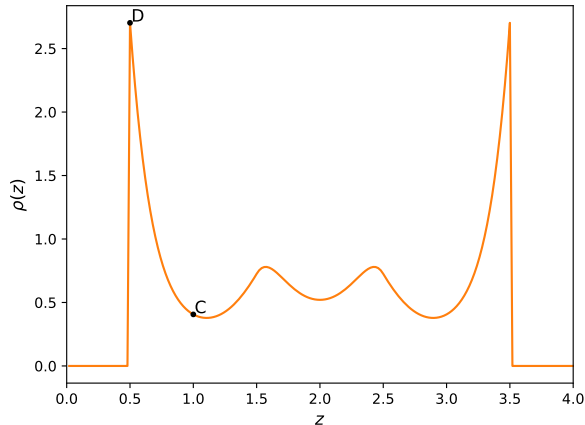


FIG. 7. **Confined hard-sphere system.** Density profile for $\mu = 5$ (solid line). Points indicate the z -coordinates for which we show the total correlation function in Fig.8.

tact peak of the profile, we find more substantial differences between the two approaches. The amplitude of the oscillations predicted by the FMT are somewhat larger than those from the PY theory, but the overall level of agreement remains satisfactory. For separations $r > 2.75$ the predictions of PY theory and the FMT become very similar.

Spherical geometry

As a test of our analytic FMT formulae in spherical geometry we will use the inhomogeneous total correlation function to calculate the three-body correlations of the bulk fluid. This can be achieved by extending the test-particle idea of Percus [2] to the two-body level. If we specify the external field to represent a hard-sphere fixed at the coordinate origin, then the inhomogeneous correlation function $g_{\text{hs}}^{tp}(\mathbf{r}_1, \mathbf{r}_2) \equiv h_{\text{hs}}^{tp}(\mathbf{r}_1, \mathbf{r}_2) + 1$ is related to the *bulk* triplet correlation function according to

$$g^{(3)}(r_1, r_2, r_{12}) = \frac{\rho^{tp}(r_1)\rho^{tp}(r_2)g^{tp}(\mathbf{r}_1, \mathbf{r}_2)}{\rho_b^2}, \quad (59)$$

where we employ the superscript *tp* to indicate functions calculated in the presence of a test-particle at the origin. Experience with triplet correlations has shown that direct analysis of $g^{(3)}$ is not the best choice when seeking to assess the quality of a given approximation. A better option is the following function

$$\Gamma(r_1, r_2, r_{12}) = \frac{\rho_b^3 g^{(3)}(r_1, r_2, r_{12})}{\rho^{tp}(r_1)\rho^{tp}(r_2)\rho^{tp}(r_{12})}, \quad (60)$$

which scales the triplet correlation function by the well-known Kirkwood superposition approximation [15]. Deviations of Γ from unity thus provide a sensitive measure of nontrivial contributions to the three-body correlations.

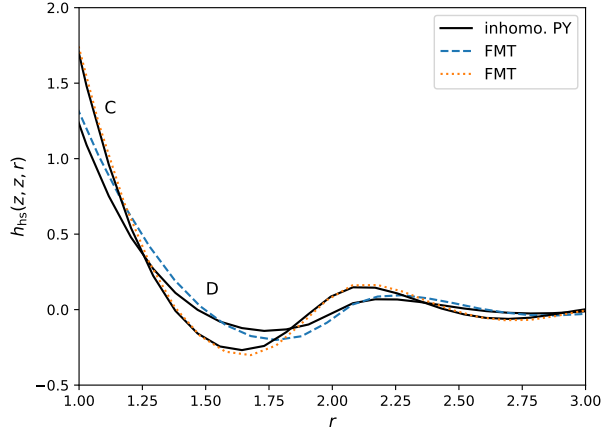


FIG. 8. **Confined hard-sphere system.** Two-body direct correlation function corresponding to Fig.7 density profile. Inhomogeneous PY solutions (solid black lines) and FMT for $z = 0.5$ (dashed blue line) and for $z = 1$ (dotted orange line). We observe close agreement between FMT and PY theory at point C, but deviations between the two theories emerge at point D.

In Fig.9 we show the function Γ generated by FMT for ‘rolling contact’ configurations at bulk densities $\rho_b = 0.3, 0.5$ and 0.7 (marked A, B and C, respectively, in the figure). These configurations are where the Kirkwood superposition (independent probability) approximation is most severely tested, but are also of central importance in kinetic theories for the transport properties of hard-spheres (see e.g. [16, 17]). The FMT predictions are compared with Monte-Carlo simulation data taken from Refs. [18] and [19]. For the two lower bulk densities considered (points A and B) we find a good level of agreement between FMT and simulation. However, at $\rho_b = 0.7$ discrepancies emerge and the FMT prediction for the amplitude and position of the peak is less accurate. This suggests that we are approaching the limit at which the FMT two-body correlations can be considered reliable.

To investigate further this breakdown at high densities we compare in Fig.10 the predictions of FMT with simulation data for a more varied selection of configurations at the even higher density, $\rho_b = 0.8$. Panel A shows the variation for a rolling contact configuration. An unphysical ‘shoulder’, already visible in panel C of Fig.9, becomes more pronounced, although one could argue that the overall description remains acceptable. This shoulder feature becomes more prominent when considering a rolling configuration with slightly more separation between the particles, shown in panel B of Fig.10. Despite showing reasonable behaviour at larger separations, for $r < 2$ the description of the simulation data is rather poor. Panels C and D focus on stretched isosceles triangle configurations, which also serve to expose deficiencies of the FMT. While it is apparent that the general trends of the simulation data are roughly captured, the amplitude of

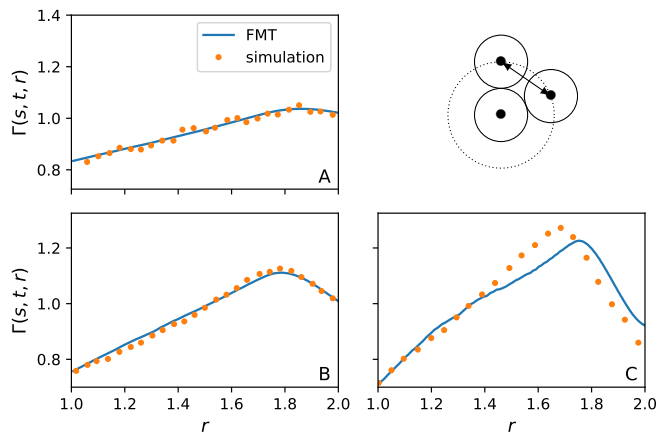


FIG. 9. **Hard-sphere triplet correlations.** Comparison of FMT (lines) with simulation data (points) [18, 19] for the quantity $\Gamma(1, 1, r)$ at $\rho_b = 0.3$ (A), 0.5 (B) and 0.7 (C). We consider rolling contact configurations for which the separation r is indicated by an arrow in the sketch.

oscillation is significantly overestimated. It would appear that the FMT performs best for rolling contact situations but leaves much to be desired at intermediate particle separations, at least for densities $\rho_b > 0.7$. It seems to us that the overall level of agreement of the FMT predictions with the Monte-Carlo data is on a similar level to that of earlier theories of the triplet correlation, such as those of Haymet *et al.* [20] and Barrat *et al.* [21]. For some examples of this we refer the reader to Fig.9 of the paper by Bilstein and Kahl [19].

V. PERTURBATION THEORY

The hard-sphere model is not sufficient to capture all of the phenomena exhibited by real fluids. An improved description can be achieved if we supplement the hard-sphere repulsion with an attractive component to the interaction potential, $u = u_{\text{hs}} + u_{\text{att}}$. If the attraction is sufficiently weak and long ranged, then the following first-order perturbation theory provides a good approximation to the Helmholtz free energy

$$F_{\text{BH}}[\rho] = F_{\text{hs}}[\rho] + \frac{1}{2} \int d\mathbf{r}_1 \int d\mathbf{r}_2 \rho(\mathbf{r}_1) \rho(\mathbf{r}_2) u^{\text{att}}(r_{12}) (1 + h_{\text{hs}}(\mathbf{r}_1, \mathbf{r}_2; [\rho])), \quad (61)$$

where the first term is the Helmholtz free energy of hard-spheres, including the ideal gas contribution. The density enters equation (61) both explicitly, via the quadratic product in the integrand, and implicitly, via the functional dependence of the hard-sphere Helmholtz free energy and total correlation function. In bulk, equation (61) reduces to the well-known first-order perturbation theory of Barker and Henderson [22–24]. For this reason the approximation (61) has been called the Barker-Henderson (BH) functional.

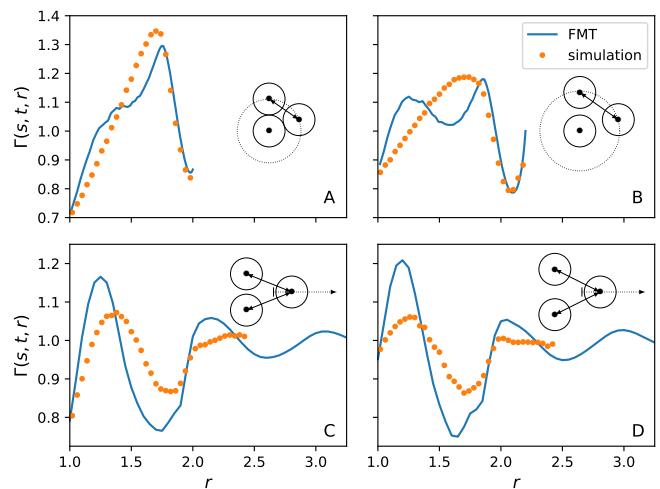


FIG. 10. **Hard-sphere triplet correlations.** Comparison of the FMT (lines) with simulation data (points) [18] for the quantity $\Gamma(s, t, r)$ at $\rho_b = 0.8$. Configurations are sketched in each figure. The separation r is indicated by the bold arrow. A and B are rolling geometries at $s = t = 1.0$ and $s = t = 1.1$, respectively. C and D are isosceles triangle configurations with $s = r$ and the base length of the triangle fixed at $t = 1.1$ and 1.3 , respectively.

In Ref.[11] we investigated the density obtained from numerical minimization of the BH grand potential (using equations (1), (3) and (61)) and found excellent agreement with simulation data for several inhomogeneous situations. Our findings suggest that the BH functional provides a quantitatively accurate description of inhomogeneous fluids with hard-core repulsion and weak attraction. Despite these promising results, widespread application of the BH functional, as implemented in [11], is likely to be hindered by the numerical effort required to minimize the grand potential. The strategy adopted, which we will henceforth refer to as the BH-PY approach, was to use FMT to approximate the first (reference) term in (61) and to obtain h_{hs} by iteratively solving the inhomogeneous PY theory (equations (8) and (14)). Clearly, using the numerical solution of an inhomogeneous integral equation theory as part of a self-consistent minimization scheme is computationally expensive, particularly when larger systems are required (e.g. studies of the liquid-vapour interface). However, we are now in a position to improve this situation by incorporating the FMT total correlation function, rather than that from the PY approximation, into (61). This BH-FMT approach yields a huge reduction in computation time and thus opens the door to applications which would be practically impossible using BH-PY.

We now briefly summarize the steps required to minimize the BH-FMT grand potential. Although this proceeds in much the same way as discussed in [11], there is a subtle but very important difference to be observed when evaluating the derivative contribution to the one-body direct correlation function. To limit the length of

the presentation we restrict attention to the case of planar geometry, although similar calculations in spherical geometry would pose no greater difficulty. To solve the Euler-Lagrange equation (4), we require the one-body direct correlation function (5). Using (61) to evaluate the derivative yields

$$c^{(1)} = c_{\text{hs}}^{(1)} + c_{\text{smf}}^{(1)} + c_{\text{corr}}^{(1)} + c_{\text{der}}^{(1)}, \quad (62)$$

where $c_{\text{hs}}^{(1)}$ is given by (12). The remaining terms involve integrals over the attractive interaction:

$$c_{\text{smf}}^{(1)}(\mathbf{r}_1) = - \int d\mathbf{r}_2 \rho(\mathbf{r}_2) \beta u^{\text{att}}(r_{12}), \quad (63)$$

$$c_{\text{corr}}^{(1)}(\mathbf{r}_1) = - \int d\mathbf{r}_2 \rho(\mathbf{r}_2) \beta u^{\text{att}}(r_{12}) h_{\text{hs}}(\mathbf{r}_1, \mathbf{r}_2), \quad (64)$$

$$c_{\text{der}}^{(1)}(\mathbf{r}_1) = - \int d\mathbf{r}_2 \int d\mathbf{r}_3 \frac{\rho(\mathbf{r}_2) \rho(\mathbf{r}_3) \beta u^{\text{att}}(r_{23})}{2} \frac{\delta h_{\text{hs}}(\mathbf{r}_2, \mathbf{r}_3)}{\delta \rho(\mathbf{r}_1)}. \quad (65)$$

The first of these is easy to calculate. The second contribution can be evaluated by using our analytic formulae for \bar{c}_{hs} as input to the OZ equation (17) and then transforming the resulting \bar{h}_{hs} back to real-space.

The functional derivative in (65) can be reexpressed in terms of a derivative with respect to the one-dimensional density profile

$$\frac{\delta h_{\text{hs}}(\mathbf{r}_1, \mathbf{r}_2)}{\delta \rho(\mathbf{r})} = \frac{1}{A} \frac{\delta h_{\text{hs}}(z_1, z_2, r)}{\delta \rho(z)}, \quad (66)$$

where A is an (arbitrary) area perpendicular to the z -axis (eliminated when performing the integrals in (65)). Using finite differences the functional derivative becomes

$$\frac{\delta h_{\text{hs}}(\mathbf{r}_1, \mathbf{r}_2)}{\delta \rho(\mathbf{r})} = \lim_{\varepsilon \rightarrow 0} \frac{h_{\text{hs}}^{\varepsilon z}(z_1, z_2, r) - h_{\text{hs}}(z_1, z_2, r)}{A\varepsilon}, \quad (67)$$

where $h_{\text{hs}}^{\varepsilon z}$ is the total correlation function evaluated at the perturbed density $\rho_z(z_3) = \rho(z_3) + \varepsilon \delta(z_3 - z)$. Substitution of the perturbed density into the transformed OZ equation (17) yields

$$\begin{aligned} \bar{h}_{\text{hs}}^{\varepsilon z}(z_1, z_2, k) &= \int_{-\infty}^{\infty} dz_3 \bar{h}_{\text{hs}}^{\varepsilon z}(z_1, z_3, k) \rho(z_3) \bar{c}_{\text{hs}}^{(2), \varepsilon z}(z_3, z_2, k) \\ &+ \bar{c}_{\text{hs}}^{(2), \varepsilon z}(z_1, z_2, k) + \varepsilon \bar{h}_{\text{hs}}^{\varepsilon z}(z_1, z, k) \bar{c}_{\text{hs}}^{(2), \varepsilon z}(z, z_2, k). \end{aligned} \quad (68)$$

Before solving (68) for $\bar{h}_{\text{hs}}^{\varepsilon z}$ we evaluate the perturbed function $\bar{c}_{\text{hs}}^{(2), \varepsilon z}$ using our analytical results. Since the Hankel transformed two-body direct correlation function depends on the density only through the weighted densities in $\Phi_{\alpha\beta}'$, the perturbed pair direct correlation function can be obtained simply by substituting perturbed weighted densities, $n_{\alpha}^{\varepsilon z}$, into $\Phi_{\alpha\beta}'$. In planar geometry the weighted densities can be expressed as

$$n_{\alpha}(z_1) = \int dz_2 \rho(z_2) \omega_{\alpha}(z_1 - z_2), \quad (69)$$

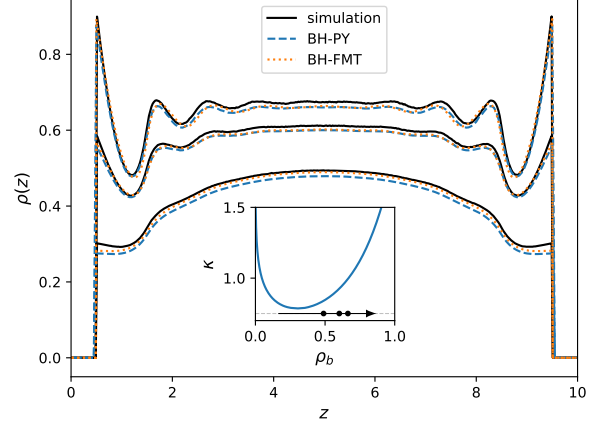


FIG. 11. **Attractive hard-spheres under confinement.** Profiles for $\mu = -2.00, -1.50$ and -1.00 , respectively, at parameter values $\kappa = 0.75$ and $\alpha = 1.8$. Simulation data (solid black lines) [11], BH-PY (dashed blue lines) and BH-FMT (dotted orange lines). The inset shows the phase diagram for $\alpha = 1.8$, where we indicate the plateau density of the calculated density profiles (black points) for fixed parameter $\kappa = 0.75$ (dashed silver line).

where the one-dimensional weight functions are given by

$$\begin{aligned} \omega_3(z) &= \pi (R^2 - z^2) \Theta(R - |z|), & \omega_2(z) &= 2\pi R \Theta(R - |z|), \\ \omega_1(z) &= \frac{\omega_2(z)}{4\pi R}, & \omega_0(z) &= \frac{\omega_2(z)}{4\pi R^2}, \\ \omega_2(z) &= 2\pi z \mathbf{e}_z \Theta(R - |z|), & \omega_1(z) &= \frac{\omega_2(z)}{4\pi R}. \end{aligned}$$

The perturbed weighted densities are therefore given by

$$n_{\alpha}^{\varepsilon z}(z_1) = n_{\alpha}(z_1) + \varepsilon \omega_{\alpha}(z_1 - z). \quad (70)$$

In [11] equation (68) was solved using the PY closure (14) on the perturbed functions $h_{\text{hs}}^{\varepsilon z}$ and $c_{\text{hs}}^{\varepsilon z}$ and solving the resulting *nonlinear* integral equation. This is much more demanding than the FMT route proposed here.

VI. RESULTS FOR THE HARD-CORE YUKAWA MODEL

In Fig.11 we show density profiles for the attractive hard-core Yukawa (HCY) model confined between two planar walls separated by a distance of ten particle diameters. In addition to a hard-core repulsion the pair interaction potential of the HCY model has an attractive contribution given by

$$u_{\text{att}}(r_{12}) = -\kappa \frac{e^{-\alpha(r_{12}-1)}}{r_{12}} \quad r_{12} \geq 1, \quad (71)$$

where κ and α are positive constants.

Fig.11 shows profiles calculated using both the BH-PY and BH-FMT for three different chemical potentials.

The theoretical predictions are compared with Monte-Carlo data taken from [11]. The inset to Fig.11 shows the bulk binodal, where the points indicate the plateau (mid-point) density of each of the considered profiles. For all three chemical potentials the BH-PY and BH-FMT are in very close agreement and provide a good description of the simulation data. This suggests that the BH-FMT approach can be used to generate highly accurate first-principles predictions for hard-core systems with a weak perturbing potential. The computational advantages of the BH-FMT over the BH-PY, in particular the use of parallel computation, make this a useful and practical approach to predict the properties of realistic inhomogeneous fluids. To give the reader some feeling for the demands involved - each of the BH-FMT profiles shown in Fig.11 required around four hours of computation time on a standard eight-core desktop machine (runtime effectively scales with the number of cores), whereas the corresponding BH-PY results each required several days.

VII. DISCUSSION

In this paper we have provided a detailed analysis of the inhomogeneous two-body correlation functions generated by FMT. Our formulae for the Hankel and Legendre transforms of the two-body direct correlation function enable rapid numerical evaluation of the real-space total correlation function and circumvent many of the usual numerical difficulties associated with iterative solution of inhomogeneous integral equation closures.

Considering hard-spheres, our developments both facilitate the study of inhomogeneous microstructure and provide a fresh line of enquiry when analyzing the FMT. Past optimization strategies have focussed on thermodynamic (zero-body) and one-body quantities. It is our view that explicit consideration of the two-body correlation functions could lead to new insight into FMT, yielding both quantitative criteria for the assessment of existing approximations as well as suggesting possible improvements. For example, it would be interesting to know the influence of either improved thermodynamics or tensorial weight functions on the predictions for the bulk triplet correlation function [10].

Using the FMT total correlation function as input to the BH perturbation theory (61) yields a computationally viable approach for models of fluids with attractive interparticle interactions. The key advantage is that within FMT the inhomogeneous two-body correlation functions can be obtained using parallel computation. This is an essential feature if density functional theory beyond the one-body level is ever to become a practical tool for the investigation of relevant and interesting phenomena. The BH-FMT approach is undoubtedly much more efficient to implement than the BH-PY theory [11] and does not appear to lead to any significant reduction in accuracy (see Fig.11), even at high density.

At first sight, this conclusion might seem to be in contradiction to the triplet correlation data presented in Figs.9 and 10, where we find generally unsatisfactory performance of FMT at higher densities. We thus make the following observations: (i) The integrand appearing in the BH free energy functional (61) is weighted by the attractive part of the pair interaction potential, which lends particular importance to configurations around $r_{12} \approx 1$. (ii) The integral in (61) runs over both \mathbf{r}_1 and \mathbf{r}_2 and represents a complicated average over the inhomogeneous total correlation function. These two features apparently lend the BH-FMT approach a certain robustness with respect to errors in the FMT hard-sphere two-body correlations and therefore open the door to many applications of the BH-FMT approach. However, only a more extensive investigation for different external fields and values of the model parameters will reveal under which conditions BH-PY and BH-FMT remain in such good agreement.

Appendix A

The nonzero derivatives of the free energy density, $\Phi'_\alpha = \partial\Phi/\partial n_\alpha$, required for calculation of the FMT one-body direct correlation function are given by

$$\begin{aligned}\Phi'_0 &= -\ln(1-n_3), & \Phi'_1 &= \frac{n_2}{1-n_3}, \\ \Phi'_2 &= \frac{n_1}{1-n_3} + \frac{3n_2^2 - 3\mathbf{n}_2 \cdot \mathbf{n}_2}{24\pi(1-n_3)^2}, \\ \Phi'_3 &= \frac{n_0}{1-n_3} + \frac{n_1n_2 - \mathbf{n}_1 \cdot \mathbf{n}_2}{(1-n_3)^2} + \frac{n_2^3 - 3n_2\mathbf{n}_2 \cdot \mathbf{n}_2}{12\pi(1-n_3)^3}, \\ \Phi'_1 &= -\frac{\mathbf{n}_2}{1-n_3}, & \Phi'_2 &= -\frac{\mathbf{n}_1}{1-n_3} - \frac{n_2\mathbf{n}_2}{4\pi(1-n_3)^2}.\end{aligned}$$

The nonzero second derivatives, $\Phi''_{\alpha\beta} = \partial^2\Phi/\partial n_\alpha\partial n_\beta$, required to calculate the two-body direct correlation function are given by

$$\begin{aligned}\Phi''_{03} &= \Phi''_{30} = \frac{1}{1-n_3}, & \Phi''_{12} &= \Phi''_{21} = \frac{1}{1-n_3}, \\ \Phi''_{13} &= \Phi''_{31} = \frac{n_2}{(1-n_3)^2}, & \Phi''_{22} &= \frac{n_2}{4\pi(1-n_3)^2}, \\ \Phi''_{23} &= \Phi''_{32} = \frac{n_1}{(1-n_3)^2} + \frac{n_2^2 - \mathbf{n}_2 \cdot \mathbf{n}_2}{4\pi(1-n_3)^3}, \\ \Phi''_{22} &= \Phi''_{22} = -\frac{\mathbf{n}_2}{4\pi(1-n_3)^2}, \\ \Phi''_{33} &= \frac{n_0}{(1-n_3)^2} + \frac{2(n_1n_2 - \mathbf{n}_1 \cdot \mathbf{n}_2)}{(1-n_3)^3} + \frac{n_2^3 - 3n_2\mathbf{n}_2 \cdot \mathbf{n}_2}{4\pi(1-n_3)^4}, \\ \Phi''_{31} &= \Phi''_{13} = -\frac{\mathbf{n}_2}{(1-n_3)^2}, \\ \Phi''_{32} &= \Phi''_{23} = -\frac{\mathbf{n}_1}{(1-n_3)^2} - \frac{n_2\mathbf{n}_2}{2\pi(1-n_3)^3}, \\ \Phi''_{12} &= \Phi''_{21} = -\frac{1}{1-n_3}\mathbb{1}, & \Phi''_{22} &= -\frac{n_2}{4\pi(1-n_3)^2}\mathbb{1},\end{aligned}$$

where $\mathbb{1}$ is the unit tensor.

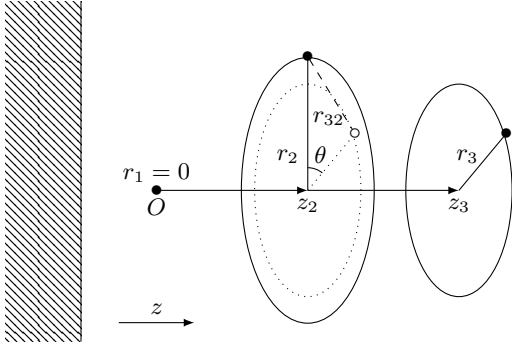


FIG. 12. Sketch of the geometry used to rewrite the OZ equation in planar geometry. The point O indicates the origin of the cylindrical coordinate system ($z_1 = 0, r_1 = 0$).

Appendix B

We show how to obtain the Hankel transformed OZ equation for planar geometry (17) starting from the general expression (8). To clarify the treatment of ‘class 3’ terms in the main text we find it convenient to break the calculation into two steps.

Step 1: When the density has a planar geometry we can express the OZ equation (8) in the cylindrical coordinate system

$$h(z_1, z_2, r_2) = c^{(2)}(z_1, z_2, r_2) + \int_{-\infty}^{\infty} dz_3 \int_0^{2\pi} d\theta \quad (\text{B1}) \\ \times \int_0^{\infty} dr_3 r_3 h(z_1, z_3, r_3) \rho(z_3) c^{(2)}(z_3, z_2, r_{32}).$$

In Fig.12 we specify the geometry. If we choose z_1 as the axis of our cylindrical coordinates, then the z -projected separation between the points at \mathbf{r}_2 and \mathbf{r}_3 is given by $r_{32} = \sqrt{r_2^2 + r_3^2 - 2r_2 r_3 \cos(\theta)}$. The Hankel back-transform of the pair direct correlation function (16) and the total correlation function can be expressed as

$$c^{(2)}(z_1, z_2, r) = \frac{1}{(2\pi)^2} \int d\mathbf{k} J_0(kr) \bar{c}^{(2)}(z_1, z_2, k), \quad (\text{B2})$$

$$h(z_1, z_2, r) = \frac{1}{(2\pi)^2} \int d\mathbf{k} J_0(kr) \bar{h}(z_1, z_2, k), \quad (\text{B3})$$

where $d\mathbf{k}$ is an area element in the plane orthogonal to the z -axis. Substitution of (B2) and (B3) into (B1) yields

$$h(z_1, z_2, r_2) = \quad (\text{B4}) \\ c^{(2)}(z_1, z_2, r_2) + \frac{1}{(2\pi)^4} \int_{-\infty}^{\infty} dz_3 \rho(z_3) \int_0^{\infty} dr_3 r_3 \int d\mathbf{k}' \int d\mathbf{k}'' \\ \times \bar{h}(z_1, z_3, k') \bar{c}^{(2)}(z_3, z_2, k'') J_0(k' r_3) \int_0^{2\pi} d\theta J_0(k'' r_{32}),$$

where we note that the separation r_{32} is a function of θ .

Graf’s addition theorem for Bessel functions states that

$$J_0(r_{23}) = \sum_{n=-\infty}^{\infty} J_n(r_2) J_n(r_3) e^{in\theta}, \quad (\text{B5})$$

which implies the useful result

$$\int_0^{2\pi} d\theta J_0(r_{23}) = 2\pi J_0(r_2) J_0(r_3). \quad (\text{B6})$$

Using (B6) to perform the θ -integral in (B4) yields

$$h(z_1, z_2, r_2) = c^{(2)}(z_1, z_2, r_2) + \int_{-\infty}^{\infty} dz_3 \rho(z_3) \\ \times \int d\mathbf{k}' \int d\mathbf{k}'' \bar{h}(z_1, z_3, k') \bar{c}^{(2)}(z_3, z_2, k'') J_0(k'' r_2) \\ \times \frac{1}{(2\pi)^3} \int_0^{\infty} dr_3 r_3 J_0(k' r_3) J_0(k'' r_3). \quad (\text{B7})$$

Bessel functions obey the orthogonality relation

$$2\pi \int_0^{\infty} dr_3 r_3 J_0(kr_3) J_0(k' r_3) = (2\pi)^2 \delta(\mathbf{k} - \mathbf{k}'), \quad (\text{B8})$$

which could also be viewed as the Hankel transform of the zero-order Bessel function. Using this in (B7) yields

$$h(z_1, z_2, r_2) = c^{(2)}(z_1, z_2, r_2) + \int_{-\infty}^{\infty} dz_3 \rho(z_3) \quad (\text{B9}) \\ \times \frac{1}{(2\pi)^2} \int d\mathbf{k}' \bar{h}(z_1, z_3, k') \bar{c}^{(2)}(z_3, z_2, k') J_0(k' r_2).$$

Step 2: Now that we have reexpressed the integration over the internal coordinate \mathbf{r}_3 we will Hankel transform (B9) with respect to the external coordinate r_2 . Applying the operator $2\pi \int_0^{\infty} dr_2 r_2 J_0(kr_2)$ to both sides of the equation yields

$$\bar{h}(z_1, z_2, k) = \bar{c}^{(2)}(z_1, z_2, k) + \frac{1}{2\pi} \int_{-\infty}^{\infty} dz_3 \rho(z_3) \quad (\text{B10}) \\ \times \int d\mathbf{k}' \bar{h}(z_1, z_3, k') \bar{c}^{(2)}(z_3, z_2, k') \int_0^{\infty} dr_2 r_2 J_0(kr_2) J_0(k' r_2).$$

Using once more the orthogonality relation (B8) then leads directly to the Hankel transformed OZ equation (17) in the main text.

Appendix C

We show here the calculation analogous to that in the preceding Appendix, but now for spherical geometry. Starting from the general expression (8) we obtain the Legendre transformed OZ equation (37) (closely following the presentation of Refs.[6] and [13]). To clarify the treatment of ‘class 3’ terms in the main text we break the calculation into two steps.

Step 1: The OZ equation (8) can be rewritten as

$$h(r_1, r_2, x_2) = c^{(2)}(r_1, r_2, x_2) + \int_0^\infty dr_3 r_3^2 \rho(r_3) \quad (\text{C1})$$

$$\times \int_0^{2\pi} d\phi_3 \int_{-1}^1 dx_3 h(r_1, r_3, x_3) c^{(2)}(r_3, r_2, x_3),$$

where we have chosen the z -axis of the spherical coordinate system to coincide with the vector \mathbf{r}_1 , which implies $\theta_1 = \phi_1 = 0$. Without loss of generality we can also orient the coordinates such that \mathbf{r}_2 lies in the xz -plane, such that $\phi_2 = 0$. Using the back-transform (36) to represent both the pair direct and total correlation functions yields

$$h(r_1, r_2, x_2) = c^{(2)}(r_1, r_2, x_2) + \sum_{i,j=0}^\infty \int_0^\infty dr_3 r_3^2 \rho(r_3)$$

$$\times \int_0^{2\pi} d\phi_3 \int_{-1}^1 dx_3 \hat{h}(r_1, r_3, i) \hat{c}^{(2)}(r_3, r_2, j) P_i(x_3) P_j(x_3). \quad (\text{C2})$$

For our chosen orientation of coordinate system the addition theorem for spherical harmonics states that

$$P_j(x_{32}) = P_j(x_3) P_j(x_2) \quad (\text{C3})$$

$$+ 2 \sum_{m=1}^j \frac{(i-m)!}{(j+m)!} P_j^m(x_3) P_j^m(x_2) \cos(m\phi_3).$$

Substitution of (C3) into (C2) and performing the inte-

gration over ϕ_3 yields

$$h(r_1, r_2, x_2) = c^{(2)}(r_1, r_2, x_2) + \sum_{i,j=0}^\infty \int_0^\infty dr_3 r_3^2 \rho(r_3)$$

$$\times 2\pi \int_{-1}^1 dx_3 \hat{h}(r_1, r_3, i) \hat{c}^{(2)}(r_3, r_2, j) P_i(x_3) P_j(x_3) P_j(x_2). \quad (\text{C4})$$

Legendre polynomials obey the orthogonality relation

$$\int_{-1}^1 dx P_i(x) P_j(x) = \frac{2}{2i+1} \delta_{ij}, \quad (\text{C5})$$

where δ_{ij} is the Kronecker delta. Using this in (C4) yields

$$h(r_1, r_2, x_2) = c^{(2)}(r_1, r_2, x_2) + \sum_{j=0}^\infty \int_0^\infty dr_3 r_3^2 \rho(r_3)$$

$$\times \frac{4\pi}{2j+1} \hat{h}(r_1, r_3, j) \hat{c}^{(2)}(r_3, r_2, j) P_j(x_2). \quad (\text{C6})$$

Step 2: Legendre transform (C6) with respect to the external coordinate x_2 . Applying the operator $\frac{2n+1}{2} \int_{-1}^1 dx_2 P_n(x_2)$ to both sides of the equation yields

$$\hat{h}(r_1, r_2, n) = \hat{c}^{(2)}(r_1, r_2, n) + \sum_{j=0}^\infty \int_0^\infty dr_3 r_3^2 \rho(r_3) 2\pi \quad (\text{C7})$$

$$\times \frac{2n+1}{2j+1} \hat{h}(r_1, r_3, j) \hat{c}^{(2)}(r_3, r_2, j) \int_{-1}^1 dx_2 P_n(x_2) P_j(x_2).$$

Using once more the orthogonality relation (C5) then leads directly to the Legendre transformed OZ equation (37) in the main text.

-
- [1] R. Evans, *Advances in Physics* **28**, 143 (1979).
[2] R. Evans, in *Fundamentals of Inhomogeneous Fluids*, edited by D. Henderson (Dekker, New York, 1992).
[3] J. S. Rowlinson and B. Widom, *Molecular Theory of Capillarity* (Dover, 2003).
[4] J. P. Hansen and I. R. McDonald, *Theory of Simple Liquids* (Elsevier Science, 2006).
[5] C. Caccamo, *Physics Reports* **274**, 1 (1996).
[6] P. Attard, *The Journal of Chemical Physics* **91**, 3072 (1989).
[7] J. M. Brader, *J.Chem.Phys* **128**, 104503 (2008).
[8] I. Omelyan, F. Hirata, and A. Kovalenko, *PCCP* **7**, 4132 (2005).
[9] Y. Rosenfeld, *Phys. Rev. Lett.* **63**, 980 (1989).
[10] R. Roth, *Journal of Physics: Condensed Matter* **22**, 063102 (2010).
[11] S. M. Tschopp, H. D. Vuijk, A. Sharma, and J. M. Brader, *Phys. Rev. E* **102**, 042140 (2020).
[12] P. Tarazona, *Phys. Rev. Lett.* **84**, 694 (2000).
[13] P. Attard, *Thermodynamics and Statistical Mechanics: Equilibrium by Entropy Maximisation* (Elsevier Science, 2002).
[14] J. J. Sakurai, *Modern quantum mechanics* (Pearson, 1993).
[15] J. G. Kirkwood, *J.Chem.Phys.* **3**, 300 (1935).
[16] I. M. de Schepper, M. H. Ernst, and E. G. D. Cohen, *J.Stat.Phys.* **25**, 321 (1981).
[17] J. A. Leegwater and H. van Beijeren, *J.Stat.Phys.* **57**, 595 (1989).
[18] E. A. Müller and K. E. Gubbins, *Mol.Phys.* **80**, 91 (1993).
[19] B. Bildstein and G. Kahl, *J. Chem. Phys.* **100**, 5882 (1994).
[20] A. J. D. Haymet, S. A. Rice, and W. G. Madden, *J. Chem. Phys.* **74**, 3033 (1981).
[21] J.-L. Barrat, J.-P. Hansen, and G. Pastore, *Phys. Rev. Lett.* **22**, 2075 (1987).
[22] J. A. Barker and D. Henderson, *J.Chem.Phys.* **47**, 2856 (1967).
[23] J. A. Barker and D. Henderson, *J.Chem.Phys.* **47**, 4714 (1967).
[24] J. A. Barker and D. Henderson, *Rev.Mod.Phys.* **48**, 587 (1976).